MASS TRANSFER FROM GAS BUBBLES TO IMPINGING FLOW OF BIOLOGICAL FLUIDS WITH CHEMICAL REACTION

WEN-JEI YANG, R. ECHIGO, D. R. WOTTON, J. W. OU, *and* J. B. HWANG

From the Department of Mechanical Engineering, The University of Michigan, Ann Arbor, Michigan 48104. Dr. Echigo's present address is Kyusha University, Kyusha, Japan. Dr. Ou's present address is Gonzaga University, Spokane, Washington 99202.

ABSTRACT The rates of mass transfer from a gas bubble to an impinging flow of a biological fluid such as whole blood and plasma are investigated analytically and experimentally. Gases commonly found dissolved in body fluids are included. Consideration is given to the effects of the chemical reaction between the dissolved gas and the liquid on the rate of mass transfer. Through the application of boundary layer theory the over-all transfer is found to be $Sh/(Re)^{1/2} = 0.845\ Sc^{1/3}$ in the absence of chemical reaction, and $Sh/(Re)^{1/2} = F'(0)$ in the presence of chemical reaction, where Sh, Re, and Sc are the Sherwood, Reynolds, and Schmidt numbers, respectively, and $F'(0)$ is a function of Sc and the dimensionless reaction rate constant. Analytical results are also obtained for the bubble lifetime and the bubble radius-time history. These results, which are not incompatible with experimental results, can be applied to predict the dissolution of the entrapped gas emboli in the circulatory system of the human body.

NOMENCLATURE

a, b Constants.
C Mass concentration.
C_s Saturated mass concentration.
C_w Mass concentration at wall.
C_∞ Mass concentration at infinity.
d Characteristic length.
D Diffusion coefficient.
$F(\eta)$ Normalized concentration function ($=[C - C_\infty]/[C_s - C_\infty]$).
$f(\eta)$ Universal velocity function as defined by equation 9.
h Mass transfer coefficient.
k Rate constant of first-order chemical reaction.
K k/a.

m Mass of bubble.
P Liquid pressure.
P_0 Stagnation pressure.
R_1 Major semiaxis of ellipsoidal body of revolution.
R_2 Minor semiaxis of ellipsoidal body of revolution.
Re Reynolds number, $2U_\infty R/\nu$.
R Bubble radius.
R_0 Initial bubble radius.
r Coordinate.
S Surface area of bubble.
Sc Schmidt number, ν/D.
Sh Sherwood number, $2hR/D$.
t Time.
U Potential velocity in r direction.
U_∞ Free stream velocity.
u Viscous velocity in r direction.
V Volume of bubble.
W Potential velocity in z direction.
w Viscous velocity in z direction.
z Coordinate.
δ Boundary layer thickness.
η Similarity variable.
ν Kinematic viscosity.
ρ Gas density.
τ Bubble lifetime.
ψ Stream function.

INTRODUCTION

Neglecting the translatory motion of a bubble, Epstein and Plesset (1) have found approximate solutions for the rate of solution by diffusion of a gas bubble in an undersaturated or oversaturated liquid-gas solution. The effects of chemical reaction on the rates of mass transfer have been examined by Yang (2) with applications to the dissolution or growth of gas bubbles in biological fluids. The radius-time history of the bubble is found to be governed by

$$\frac{dR}{dt} = \frac{D(C_\infty - C_s)}{\rho}\left[\frac{1}{R} + \frac{\exp(-kt)}{(\pi Dt)^{1/2}} + \left(\frac{k}{D}\right)^{1/2} \operatorname{erf}(kt)^{1/2}\right], \qquad (1)$$

where R is the bubble radius; t, time; D, mass diffusion coefficient; k, rate constant of first-order chemical reaction; C_s, the dissolved gas concentration for a saturated solution at the system pressure and temperature; C_∞, the dissolved gas concentration at a distance from the bubble; and ρ, the density of the gas contained in the bubble. When $k = 0$, equation 1 reduces to

$$dR/dt = D(C_\infty - C_s)[1/R + 1/(\pi Dt)^{1/2}]/\rho,$$

the approximate solutions of which are found to be

$$(R/R_0)^2 = 1 \pm 2Dt/R_0^2, \tag{2}$$

where R_0 is the bubble radius at the initial time $t = 0$, the plus sign is for an oversaturated solution in which the bubble grows, and the minus sign is for an undersaturated solution in which the bubble shrinks.

When a gas bubble is in relative motion with a liquid-gas solution, the rate of mass transfer between the bubble and the solution is enhanced by convective transfer and thus the growth or collapse of the bubble is substantially accelerated. The situation corresponds to the case where the gas bubble is riding in a stream of the solution or the bubble is rising in a quiescent solution. It is known that bubbles with diameters of less than 0.01 cm rise like solid spheres in accordance with Stokes's law (3). The following two equations predict the rate of mass transfer from a solid sphere:

$$Sh = 0.37R^{0.6}Sc^{1/3} \tag{3}$$

and

$$Sh = 0.582Re^{1/2}Sc^{1/3} \tag{4}$$

are obtained by Grigull (4) and Linton and Sutherland (5), respectively. *Sh*, *Re*, and *Sc* are the Sherwood, Reynolds, and Schmidt numbers, respectively. They are defined as $Sh = 2hR/D$, $Re = 2RU_\infty/\nu$, and $Sc = \nu/D$, where h is the mass transfer coefficient between the sphere and the liquid, ν is the liquid kinetic viscosity, and U_∞ is the free stream velocity. Ruckenstein (6) has investigated the rate of heat transfer between rising vapor bubbles and a boiling liquid. Applying the analogy between heat and mass transfer, his result can be written as

$$Sh = (4/\pi)^{1/2}(ReSc)^{1/2}. \tag{5}$$

The bubble radius is found to vary as

$$(R/R_0)^{5/4} = 1 + bt, \tag{6}$$

where b is a constant.

The present paper investigates the rate of mass transfer from a gas bubble to an impinging liquid-gas solution. The bubble is situated at the stagnation point of the axisymmetrical flow of the solution. In addition to the contribution of diffusion and convection, the effects of chemical reaction between the dissolved gas and the liquid on the rate of mass transfer are taken into account. Through the application of boundary layer theory, analytical results are obtained for the rate of mass transfer, the bubble lifetime, and the bubble radius-time history. These results, confirmed

experimentally, may be used to predict the dissolution of entrapped gas emboli in the circulatory system of human body (reference 7).

ANALYSIS

A spherical gas bubble of radius R_0 at the initial time $t = 0$ is placed at the stagnation point in the axisymmetrical flow of a liquid-gas solution with the stream impinging on a wall at right angles to it and flowing away radially in all directions. The concentration of dissolved gas in the solution is uniform and equal to C_∞. The first-order chemical reaction takes place in a solution maintained at constant pressure and temperature. The dissolved gas concentration for a saturated solution at the system temperature and pressure is denoted by C_s. During the time $t > 0$ that follows the transient, a gas bubble in a solution will grow or shrink by mass transfer if the solution is oversaturated or undersaturated irrespective of the presence of chemical reaction. The purpose of the study is to determine the rate of mass transfer between the bubble and the solution and the radius-time history of the bubble.

The stagnation point will be taken as the origin of the cylindrical coordinate system (r, θ, z), with the flow in the direction of the negative z axis (Fig. 1). The radial and axial components in frictionless flow outside the laminar boundary layer over the solid wall are denoted by U and W respectively, whereas those in viscous flow inside the boundary layer are denoted by $u(r, z)$ and $w(r, z)$ respectively. Fluid mechanics texts such as Schlichting (8) state that

$$U = ar, \qquad W = -2az, \tag{7}$$

$$u = \frac{1}{r}\frac{\partial}{\partial r}(r\psi), \qquad w = -\frac{1}{r}\frac{\partial}{\partial r}(r\psi), \tag{8}$$

in which the Stokes stream function ψ and the similarity variable η are defined as

$$\psi = (a\nu)^{1/2} r f(\eta), \qquad \eta = z(a/\nu)^{1/2}, \tag{9}$$

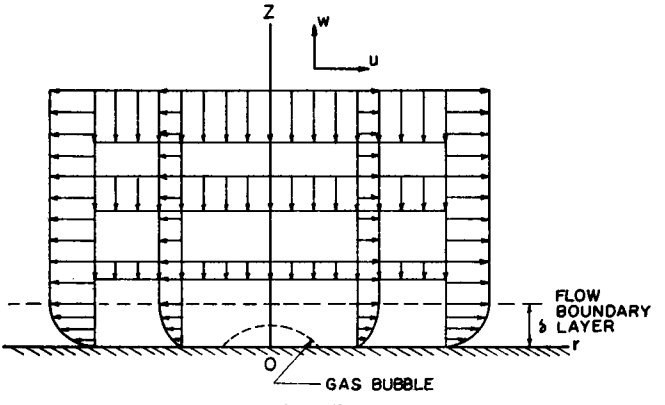

FIGURE 1 Coordinate systems.

respectively, a is a constant, and ν is the kinematic viscosity of the solution. The universal velocity distribution function $f(\eta)$ must satisfy the differential equation

$$f''' + 2ff'' - (f')^2 + 1 = 0, \tag{10}$$

subject to the boundary conditions

$$f(0) = f'(0) = 0, \qquad f'(\infty) = 1.$$

The prime denotes differentiation with respect to η. From the definition and Table 5.1 of reference 8, the boundary layer thickness in the flow is found to be 1.98 $(\nu/a)^{1/2}$.

The dissolved gas concentration $C(r, z)$ at a point in the solution near the bubble can be found using the mass transfer equation:

$$u\frac{\partial C}{\partial r} + v\frac{\partial C}{\partial z} = D\nabla^2 C - kC\,. \tag{11}$$

The concentration is C_s at the bubble surface and C_∞ in the free stream. The region around the bubble through which the diffusion process takes place is soon much larger than the bubble itself. Here one may assume that the configuration of the surrounding concentration in the solution is identical with the concentration distribution in the boundary layer over a fictitious solid wall, maintained at concentration C_s in the absence of the bubble. This postulation gives rise to the specification of the boundary conditions for equation 11 as

$$C(r, 0) = C_s\,, \qquad C(r, \infty) = C_\infty\,. \tag{12}$$

Taking C_∞ as a reference, $F(\eta)$ and K are defined:

$$F(\eta) = C(r, \theta)/C_s\,, \qquad K = k/a. \tag{13}$$

With the substitution of equations 8, 9, and 13, equation 11 reduces to the ordinary differential equation

$$F'' + Sc(2fF' - KF) = 0, \tag{14}$$

subject to the appropriate boundary conditions:

$$F(0) = 1, \qquad F(\infty) = 0.$$

$F(\eta)$ is the universal concentration distribution function obtained from the integration of equation 14. For $K = 0$ or in the absence of chemical reaction, it yields

$$F(\eta) = 1 - \left[\int_0^\eta \exp\left(-2Sc\int_0^\eta f\,d\eta\right)d\eta \Big/ \int_0^\infty \exp\left(-2Sc\int_0^\eta f\,d\eta\right)d\eta\right]. \tag{15}$$

For K other than zero, the F function must be obtained through a numerical integration of equation 14.

The rate of mass transfer from the bubble to the solution can be expressed by the Sherwood number as

$$Sh = \frac{d}{D(C_s - C_\infty)S}\frac{dm}{dt}, \tag{16}$$

where d, S, and m are the characteristic length, surface area, and mass of the bubble respectively. For a spherical bubble, $d = 2R$, $S = 4\pi R^2$, and $m = \rho 4\pi R^3/3$. In the present case the equation $dm/dt = SD(\partial C/\partial z)_{z=0}$ and equation 14 can be reduced to

$$Sh/(Re)^{1/2} = -F'(0). \tag{17}$$

In reference to the f' vs. η plot not presented here, the f' function for $K = 0$ case can be approximated as

$$f' = 1.312\eta, \tag{18}$$

in the range of small η. Accordingly, one gets from equations 15 and 17

$$Sh/(Re)^{1/2} = 0.845Sc^{1/3}. \tag{19}$$

The shape of a gas bubble in axisymmetrical flow is important. The experiments reported in the following section demonstrate that the gas bubble at the stagnation point of an axisymmetrical flow of liquid resembles a hemiellipsoidal body of revolution, with the major semiaxis R_1 approximately twice the minor semiaxis R_2. The surface area and volume of such a body can be expressed as

$$S = \pi R_1^2\left[1 + \frac{1}{2}\frac{R_2^2}{R_1(R_1^2 - R_2^2)^{1/2}}\ln\left|\frac{(R_1^2 - R_2^2)^{1/2} + R_1}{(R_1^2 - R_2^2)^{1/2} - R_1}\right|\right], \tag{20}$$

and

$$V = 2\pi R_1^2 R_2/3, \tag{21}$$

respectively. This observation has substantial theoretical support. It is known that the pressure distribution P in the potential flow portion of the axisymmetrical flow field is

$$P_0 - P = \rho_l(U^2 + W^2)/2 = \rho_l a^2(r^2 + 4z^2)/2, \tag{22}$$

in which P_0 is the liquid stagnation pressure and ρ_l is the liquid density. Hence, a constant pressure surface is described by

$$\rho_l a^2(r^2 + 4z^2)/2 = \text{const.}$$

This equation also describes a hemiellipsoidal body of revolution with $R_1 = 2R_2$.

The pressure distribution in the flow boundary layer is

$$P_0 - P = \rho_l a^2[r^2 + \nu g(\eta)/a]/2, \tag{23}$$

where the function $g(\eta)$ must satisfy the differential equation

$$f''' + 2ff' - g'(\eta)/4 = 0,$$

subject to the boundary condition $g(0) = 0$. Utilizing the approximation $f' = 1.312$ the function $g(\eta)$ is found to be approximately 5.25η or $5.25z(a/\nu)^{1/2}$. Hence, the constant pressure surface described by equation 23 is a hemiellipsoidal body of revolution, although R_1 is not precisely $2R_2$. This conclusion is confirmed experimentally.

Knowing bubble shape, one can then determine the radius-time history of the gas bubble. With the aid of equations 17, 20, and 21 for $R_1 = 2R_2$, the simple mass balance at bubble surface,

$$\mathrm{d}(\rho V)/\mathrm{d}t = SD(\partial C/\partial z)_{z=0}, \tag{24}$$

produces

$$-\frac{\mathrm{d}R_1}{\mathrm{d}t} = \left[1 + \frac{1}{4(3)^{1/2}} \ln \frac{2 + (3)^{1/2}}{2 - (3)^{1/2}}\right] \frac{D}{\rho} (C_s - C_\infty) \left(\frac{a}{\nu}\right)^{1/2} F'(0). \tag{25}$$

Integrating the last equation with the initial condition $R_1(0) = R_0$ yields

$$\frac{R_1(t)}{R_0} = 1 - \left[1 + \frac{1}{4(3)^{1/2}} \ln \frac{2 + (3)^{1/2}}{2 - (3)^{1/2}}\right] \frac{D(C_s - C_\infty)}{\rho} \left(\frac{a}{\nu}\right)^{1/2} F'(0)t, \tag{26}$$

from which the lifetime of the bubble is found to be

$$\frac{\tau}{2R_0} = \left\{\left[1 + \frac{1}{4(3)^{1/2}} \ln \frac{2 + (3)^{1/2}}{2 - (3)^{1/2}}\right] \frac{D(C_s - C_\infty)}{\rho} \left(\frac{a}{\nu}\right)^{1/2} F'(0)\right\}^{-1}. \tag{27}$$

In the absence of chemical reaction, equations 26 and 27 reduce to

$$\frac{R_1}{R_0} = 1 - \left\{\frac{6(0.414)^{1/3}}{\Gamma(1/3)} \left[1 + \frac{1}{4(3)^{1/3}} \ln \frac{2 + (3)^{1/2}}{2 - (3)^{1/2}}\right] \frac{D(C_s - C_\infty)}{2\rho R_0} \left(\frac{a}{\nu}\right)^{1/2} Sc^{1/3}\right\} t, \tag{28}$$

and

$$\frac{\tau}{2R_0} = \left\{\frac{6(0.414)^{1/3}}{\Gamma(1/3)} \left[1 + \frac{1}{4(3)^{1/3}} \ln \frac{2 + (3)^{1/2}}{2 - (3)^{1/2}}\right] \frac{D(C_s - C_\infty)}{\rho} \left(\frac{a}{\nu}\right)^{1/2} Sc^{1/3}\right\}^{-1}, \tag{29}$$

respectively.

The function $F(\eta)$ is evaluated by integrating equation 14 using an IBM 360 digital computer. The result, presented graphically in Fig. 2, shows that the gradient of the function becomes steeper with an increase in K, indicating either an increase in the rate of mass transfer from the gas bubble or a rapid shrinkage of the bubble as the reaction rate constant increases. Utilizing $F'(0)$, obtained from the numerical integration of equation 14, mass transfer performance described by equation 17 is plotted in Fig. 3. Equation 19 is included for comparison. The data can be fitted to

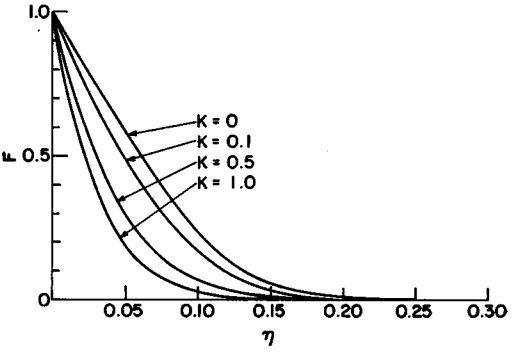

FIGURE 2 Concentration distribution in the laminar boundary layer of the axisymmetrical stagnation flow with chemical reaction for $Sc = 1000$.

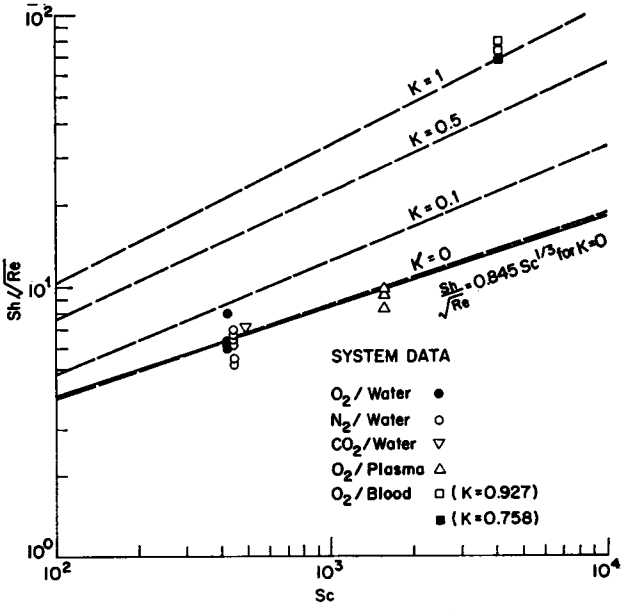

FIGURE 3 Data and theory for mass transfer from gas bubbles to water, plasma, and blood (dotted lines, numerical results of the power series solution; solid line, approximate solution, equation 17).

the expression

$$Sh/Re^{1/2} = b(Sc)^n,$$

where $b = 0.773, 0.71, 0.881, 0.97$ and $n = 0.351, 0.415, 0.470, 0.513$ for $K = 0, 0.1, 0.5, 1.0$, respectively. In the absence of chemical reaction, equation 19, obtained by approximating the f' function, agrees very well with equation 15, derived using the power series expansion.

Fig. 3 also shows the effect of the parameter K on mass transfer performance. The reaction rate constant k is 9.76 sec^{-1} for oxygen bubbles in whole blood and 0.025 sec^{-1} for carbon dioxide bubbles in water, according to Roughton (9). For a physical system with specified k, however, the dimensionless quantity K may take many different values depending upon the magnitude of the velocity constant in a laminar flow range. Generally speaking, mass transfer performance is greatly improved with an increase in K, as indicated by a substantial increase in the Sherwood number in Fig. 3.

An examination of both equations 26 and 28 shows that the bubble radius varies as a linear function of time. This is in contrast to the results of the previous studies which show that a stationary bubble would grow or shrink as a square root function of time according to equation 2, while the size of a bubble rising in a liquid would vary as a 4/5 power function of time as illustrated by equation 6. More rapid collapse

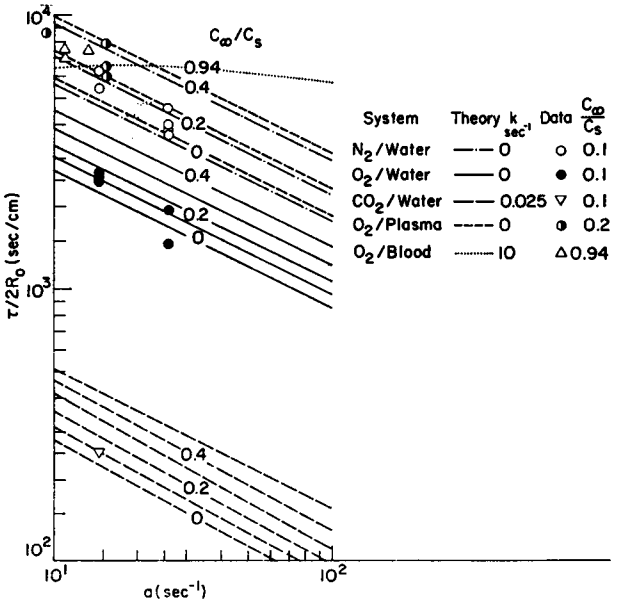

FIGURE 4 Comparison between theory and experimental results for the lifetime of nitrogen, oxygen, and carbon dioxide bubbles in degassed water and of oxygen bubbles in degassed plasma and whole blood.

or growth of gas bubbles in the present study is due to greater contribution of convective component to mass transfer in the axisymmetrical stagnation flow case.

Equation 29, giving the lifetime of the bubble for the case of $K = 0$, is plotted in Fig. 4 for nitrogen, oxygen, and carbon dioxide bubbles in water and oxygen bubbles in plasma and whole blood for various values of C_∞/C_s. As expected, the bubble lifetime is extended as the value of C_∞/C_s increases, but is shortened as the impinging velocity increases.

EXPERIMENTAL APPARATUS

The test apparatus used in this experiment is depicted in Fig. 5. The liquid reservoir (1) consists of two concentric Plexiglas tubes of different heights, a taller inner tube and shorter outer tube, both mounted on a flat Plexiglas sheet. A series of appropriately spaced ¼-inch-diameter holes are drilled on two opposite sides of the shorter tube and the upper portion of the taller tube. By plugging some of the holes, two different liquid levels can be created in the reservoir: a higher liquid level in the taller tube and a lower one in the shorter tube. A brass tube covered with a Plexiglas sheet is then mounted over the two concentric Plexiglas tubes. This serves as an evacuation chamber (2) for the fluid reservoir. A Sarns 3500 model roller pump (3) (Sarns, Inc., Ann Arbor, Mich.) is used to circulate the liquid, which is spilled over the reservoir on the chamber floor back into the taller Plexiglas tube of the reservoir.

Two condensers (7), each consisting of a flask placed in an ice bath, are connected in series to trap water vapor before it enters a Cenco Hyvac-14 vacuum pump (11) (Cenco Instruments Corp., Chicago, Ill.) during the degassing of the liquid. A mercury manometer (8) is connected to a line between the evacuation chamber and the condensers. After the degassing of the liquid is completed, the space above the liquid in the evacuation chamber is filled with gaseous nitrogen drawn from a nitrogen source (9).

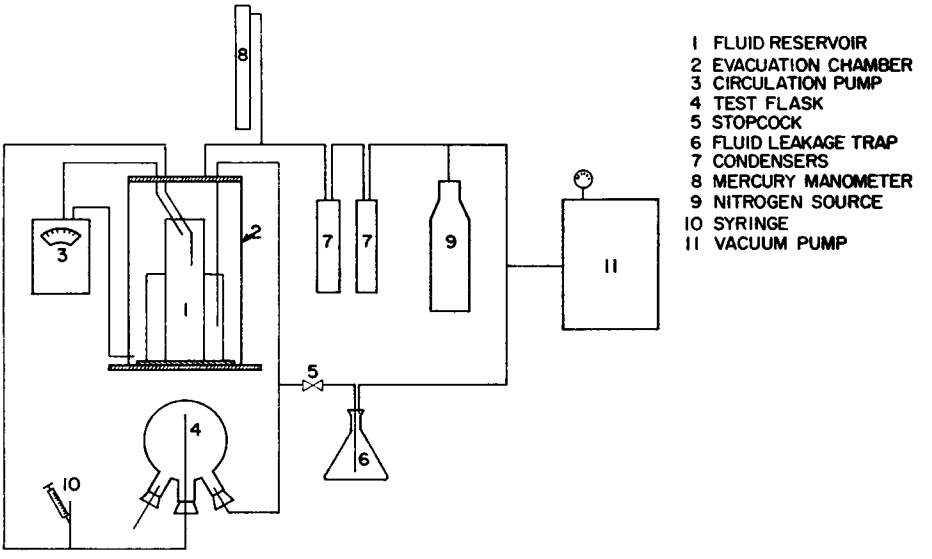

FIGURE 5 Experimental apparatus.

The test flask (4) into which the gas bubble is injected is a 250 ml Pyrex boiling flask with three openings. A 6-mm-I.D. glass tube is inserted through the stopper in the center opening until its tip is about 0.5 cm from the inner surface of the test flask. This glass tube will be used as the throat for producing a circular jet to impinge upon the gas bubble. The inner surface of the test flask in the vicinity of the tip of the glass tube is coated with a thin film of RTV adhesive (room temperature vulcanizing, Dow Chemical Co., Midland, Mich.), so that a gas bubble injected into the test flask through the liquid line will stay on the inner surface of the test flask. The liquid in the upper level inner tube in the reservoir flows into the test flask through the center opening. It then flows back to the lower level (outer tube) in the reservoir through the second opening of the test flask. The third opening is used for venting entrapped gas or vapor in the test flask. The stopcock (5) is opened during the degassing process to evacuate the test flask and connected tubing. A 250 ml Erlenmeyer flask 6 is connected with the line between the test flask and the vacuum pump to trap any fluid passing through the stopcock (5).

TEST PROCEDURE

The experiments are conducted in two steps: the degassing of blood and plasma and the injection of a gas bubble into the degassed liquid followed by the measurements of the instantaneous bubble size. After some of the holes drilled on the Plexiglas tube walls are plugged for desired liquid levels in the reservoir (1), the test flask (4) is placed at a position above the evacuation chamber (2). The stopcock (5) is then closed, followed by the closing of the tubing leading to the nitrogen source (9), with a Hoffman pinchcock (Humboldt Mfg. Co., Chicago, Ill.). The vacuum pump (11) is started. When a desired level of vacuum is established in the evacuation chamber, the stopcock is opened. The vacuum pump is turned off as soon as all evidence of "boiling" within the evacuation chamber has ceased. Then the stopcock is closed, the roller pump (3) started, and the test flask is lowered to a position below the evacuation chamber. The line leading to the nitrogen source is opened by removing the pinchcock until the system is filled with gaseous nitrogen at atmospheric pressure. When nitrogen bubbles are tested, the system is opened to atmospheric air instead of gaseous nitrogen. The gas or vapor entrapped in the test flask is vented through the third opening of the test flask.

After a small gas bubble is injected into the fluid by means of the syringe (10), the tubing leading from the evacuation chamber to the test flask is closed with a Hoffman pinchcock. Extreme precaution is taken to fill the needle on the end of the syringe with test gas so that air is not entrapped in the syringe (in the interest of brevity the method employed to fill the needle with the test gas is not included here). The bubble is then brought to rest at the top of the inverted test flask and is positioned on the axis of the jet tube, as shown in Fig. 2, by adjusting the positions of the tubing and the test flask. Upon the removal of the Hoffman pinchcock, the liquid starts to circulate in the loop between the evacuation chamber and the test flask and the jet of the liquid impinges upon the gas bubble.

The size of the gas bubble is measured by observing it through the bottom of the inverted test flask with an Edscorp comparitor (Edmund Scientific Co., Barrington, N.J.). The size of the bubble is recorded as a function of time, until its complete dissolution in the liquid. The flow rate at the given liquid level is known through the calibration of the Sarns roller pump, used to maintain the liquid level while the liquid flowed through the test flask. The viscosity of the liquid is measured before and after each test as mentioned in the first part, in order to check any possible change in the liquid property resulting from the degassing process or its continuous exposure to the room temperature and pressure.

COMPARISON OF THEORY WITH EXPERIMENTAL DATA

Typical experimental results for mass transfer from gas bubbles to the impinging liquid are shown in Fig. 3 in dimensionless form as $Sh/(Re)^{1/2}$ vs. Sc. The experimental value of a is calculated using equation 7, $a = 1 - (W/2)$, in which W is the volumetric flow rate of the liquid per unit cross-sectional area of the nozzle with 6 mm diameter, and l is the distance between the nozzle tip and the inner surface of the test flask shown in Fig. 6. For this test setup, a in seconds^{-1} is equal to the volumetric flow rate in cubic centimeters per second of the liquid through the nozzle in cubic centimeters per second divided by the flow cross-sectional area 0.283 cm^2. The liquid temperatures during the experiments are at about 20°C. The liquids are degassed for approximately 9 hr before testing. The values of K in the experiments are 1.71×10^{-3} for the CO_2/water (carbon dioxide bubble in water) system, 0.927 and 0.758 for the O_2/blood system, and zero for all other systems. The solubility of gases in liquids, C_s, is generally expressed in terms of the Bunsen absorption coefficient, which is defined as the volume of gas at standard pressure and temperature, dissolved by a unit volume of the liquid when there is a partial pressure of the gas of 1 atm. Since less than 5% of the total amount of oxygen carried by the blood is found to be in simple physical solution, a reversible chemical reaction is responsible for at least 95% of the dissolved oxygen; however, a normal value for the oxygen partial pressure P_{O_2} of arterial blood is 100 mm Hg or 100/760 atm. Hence, the total oxygen content of 100 ml of equilibrated blood at 760 mm Hg and 37°C is 0.285 ml at P_{O_2} of 95 mm Hg. Since 55% of blood is plasma, the solubility of oxygen in 100 ml of plasma is 100/55 of (0.285 ml) (760 mm Hg)/(95 mm Hg) or 4.15 ml. For an oxygen density of 1.305×10^{-3} g/cm^3, this is equivalent to $C_s = 5.42 \times 10^{-5}$ g/cm^3. It is seen in Fig. 3 that for the systems without chemical reaction, such as O_2/water, N_2/water, and O_2/plasma, the mass transfer data agree very well with the predicted values; however, in the presence of a chemical reaction, the experimental results are generally higher than those predicted.

Fig. 4 compares the theory, equations 27 and 29, and experimental results for the

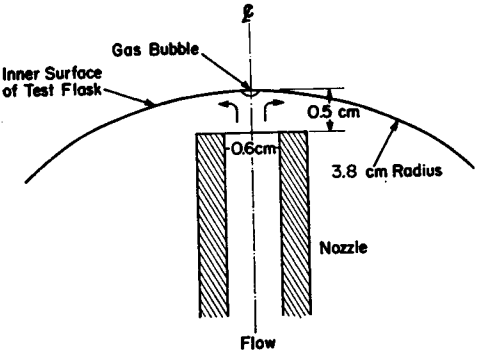

FIGURE 6 Position of gas bubble in test flask.

lifetime of the same bubbles whose mass transfer performance was plotted in Fig. 3. The values of C_∞/C_s are calculated using the readings from the vacuum pressure gage. The agreement between the theoretical predictions and the experimental data is very satisfactory for the CO_2/water system and those systems without a chemical reaction. In the case of the O_2/blood system, the data fall above the prediction. This is due to the fact that the chemical reaction between the dissolved oxygen and the reduced hemoglobin is first order only during the small times after the transient. The nature of this chemical reaction is indeed more complicated than the first-order one. The uncertainty estimations for confidence limits on the mean of 95% are evaluated for the mass transfer data in Fig. 3, and the experimental results of bubble lifetime in Fig. 4 by the method of reference 10. The 95% confidence in the mean signifies that the odds are 20 to 1 that the true value lies within the uncertainty interval. The uncertainty intervals are estimated to be 10.1 and 10% of each measurement for the experimental results of mass transfer and bubble lifetime, respectively. The reading of bubble size beneath the container surface is the major factor contributing to the uncertainty interval.

The radius-time history of all the bubbles tested is experimentally recorded but is not included in the text. It is revealed that some data indicate a linear collapse of bubbles with time, but other data exhibit a deviation from the linear relationship. Two factors contribute to this discrepancy between the theory and the data: (*a*) The equivalent bubble size is calculated from the two-dimensional measurement of a nonspherical bubble. This may contribute to an inaccuracy in data, but not to a great extent. (*b*) The initial diameter of the bubbles is approximately 1 mm, while the nozzle for flow is 6 mm in diameter and is located at a distance of 5 mm from the inner surface of the test flask. The actual flow may therefore not completely justify the analytical assumption that the flow field in the vicinity of the jet is unchanged by the presence of the bubble; however, the assumption that the bubble shape is determined by the uniform pressure distribution is confirmed by our observation that the actual bubble shape appears to be the predicted ellipsoidal body of resolution.

CONCLUSION

An analytical model is developed to determine the rate of mass transfer between a gas bubble to an impinging flow of liquids, including biological fluids such as plasma and blood. Experimental data obtained for the lifetime of a gas bubble, its collapse, and the rate of mass transfer compare favorably with the theoretical predictions. It is concluded from the study that the rate of mass transfer may be predicted by the equation

$$Sh/Re^{1/2} = 0.845Sc^{1/3}$$

in the absence of a chemical reaction in the liquid-gas solution. The available data

are correlated within a maximum deviation of $\pm 23\%$ by this equation. This deviation is acceptable in the studies of transport phenomena. When the chemical reaction is present, the right-hand side of the last equation should be replaced by the function $F'(0)$, which is a function of both the Schmidt number and the dimensionless reaction rate constant. As confirmed by experiments, the lifetime of the gas bubble can be satisfactorily predicted by the analytical solutions given by equations 27 and 29.

This research was supported by the National Heart Institute, National Institutes of Health.

Received for publication 3 November 1970 and in revised form 15 March 1971.

REFERENCES

1. EPSTEIN, P. S., and M. S. PLESSET. 1950. *J. Chem. Phys.* **18**:1505.
2. YANG, W. J. 1971. *J. Biomech.* **4**:119.
3. LEVICH, V. G. 1962. Physicochemical Hydrodynamics. Prentice-Hall, Inc., Englewood Cliffs, N. J. 395.
4. GRIGULL, V. 1955. Die Grundgesetze der Warmeubertrangung. Springer-Verlag KG, Berlin.
5. LINTON, M., and K. L. SUTHERLAND. 1960. *Chem. Eng. Sci.* **12**:214.
6. RUCKENSTEIN, E. 1959. *Chem. Eng. Sci.* **10**:22.
7. CHAN, K. S., and W. J. YANG. 1969. *J. Biomech.* **2**:299.
8. SCHLICHTING, H. 1960. Boundary Layer Theory. McGraw-Hill Book Company, New York. 66.
9. ROUGHTON, F. J. W. 1964–1965. *Handb. Physiol.* **1**:767.
10. KLINE, S. J., and F. A. MCCLINTOCK. 1953. *Mech. Eng.* **75**:3.